Title

Real-Time Unsupervised Detection of Early Damage in Railway Bridges Using Traffic-Induced Responses

ISBN

9783030817152

Authors

Meixedo, Andreia
Ribeiro, Diogo
Santos, João
et al.

Publication Date

2022

DOI

10.1007/978-3-030-81716-9_6

Peer reviewed

Real-time unsupervised detection of early damage in railway bridges using traffic-induced responses

Andreia Meixedo[1], Diogo Ribeiro[2], João Santos[3], Rui Calçada[4] and Michael Todd[5]

[1,4] CONSTRUCT-LESE, Faculty of Engineering, University of Porto, Portugal
[2] CONSTRUCT-LESE, School of Engineering, Polytechnic of Porto, Portugal
[3] LNEC, Laboratório Nacional de Engenharia Civil, Portugal
[5] Department of Structural Engineering, University California San Diego, USA
[1]ameixedo@fe.up.pt, [2]drr@isep.ipp.pt, [3] josantos@lnec.pt,
[4]ruiabc@fe.up.pt, [5] mdtodd@ucsd.edu

Abstract. This chapter addresses unsupervised damage detection in railway bridges by presenting a novel AI-based SHM strategy using traffic-induced dynamic responses. To achieve this goal a hybrid combination of wavelets, PCA and cluster analysis is implemented. Damage-sensitive features from train-induced dynamic responses are extracted and allow taking advantage not only of the repeatability of the loading, but also, of its large magnitude, thus enhancing sensitivity to small-magnitude structural changes. The effectiveness of the proposed methodology is validated in a long-span bowstring-arch railway bridge with a permanent structural monitoring system installed. A digital twin of the bridge was used, along with experimental values of temperature, noise, trains loadings and speeds, to realistically simulate baseline and damage scenarios. The methodology proved highly sensitive in detecting early damage, even in case of small stiffness reductions that do not impair structural safety, as well as highly robust to false detections. The ability to identify early damage, imperceptible in the original signals, while avoiding observable changes induced by environmental and operational variations, is achieved by carefully defining the modelling and fusion sequence of the information. A damage detection strategy capable of characterizing multi-sensor data while being sensitive to identify local changes, is proposed as a tool for real-time structural assessment of bridges without interfering with the normal service condition.

Keywords: Railway bridges, Structural Health Monitoring, traffic-induced dynamic responses, damage detection, unsupervised learning, data-driven, artificial intelligence.

1 Introduction

Modern societies are critically dependent upon transport infrastructure such as roadway or railway bridges and tunnels, which has motivated active research to reduce the costs of inspection and maintenance. A large number of bridges are nearing the end of their life cycle, and since these infrastructures cannot be economically replaced, techniques

for damage detection are being developed and implemented so that their safe operation may be extended beyond the design basis for service life. Structural health monitoring (SHM) based on Artificial Intelligence (AI) represents a promising strategy in this ongoing challenge of achieving sustainable infrastructural systems since it has the potential to identify structural damage before it becomes critical, enabling early preventive actions to be taken to minimize costs. The main goal of SHM should not be to replace the traditional inspection techniques, but to complement them with quantitative information. Proactive conservation strategies based on long-term monitoring are increasingly recommended for special structures such as long-span bridges. In fact, disruption or even the collapse of a bridge can lead to important and irreversible negative consequences for society and the economy. In short, SHM offers economical, efficient and intelligent technologies to manage the operation and maintenance of infrastructure, thereby improving safety, increasing longevity and reducing maintenance (Fig. 1).

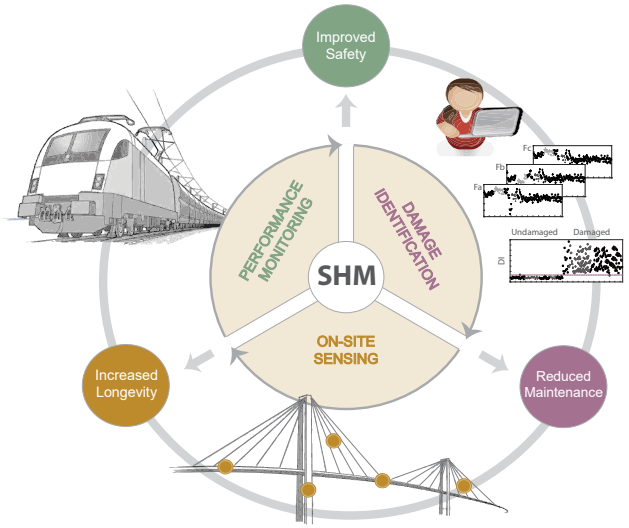

Fig. 1. Structural Health Monitoring cycle and its advantages.

SHM techniques can follow model-updating or data-driven approaches for damage detection. Model updating consists of fitting a numerical model to experimental data to infer damage-related information that cannot be directly measured on site. Despite their reported accuracy, these techniques have an inherent computational complexity, and the need for user judgement makes them less suitable for real-time SHM [1,2]. On the other hand, data-driven approaches rely on data mining techniques to extract meaningful information from time series acquired on site. The computational simplicity of these approaches renders them more attractive and cost-effective to implement online damage detection in large-scale structures.

Damage detection strategies have been widely classified by literature within a five-level hierarchy [3] i) damage detection, ii) localization, iii) type, iv) severity and v) lifetime prediction. The present chapter addresses the first level of the aforementioned

hierarchy through data-driven methods based on train-induced dynamic responses. To fulfil this goal, four main operations need to be employed after the acquisition of data: i) feature extraction, ii) feature modelling, iii) data fusion, and iv) feature classification.

Feature extraction refers to the process of transforming the time series acquired on site into an alternative information, where the correlation with the damage is more readily observed. Modal or modal-based features are the most common in the literature [4] due to the advantage of being directly associated with the mass and, more importantly, with structural stiffness, which is expected to change in the presence of damage. Nevertheless, Operational Modal Analysis (OMA)-based information can also be considered not sensitive to early damage due to the need of identifying high order modes shapes, which proves very challenging for real structure monitoring. Symbolic data [5], Continuous Wavelet Transform (CWT) [6] and autoregressive models (AR) [7] are examples of techniques successfully applied as extractors of damage-sensitive features for both static and dynamic monitoring.

Effective SHM techniques for damage detection face the challenge of distinguishing the measured effects caused by environmental and operational variations (EOVs) from those triggered by damage [8]. Hence, SHM methods that can overcome this issue must necessarily resort to feature modelling. This operation is crucial for false alarm prevention since environmental (such as temperature) and operational effects (like trains crossing at different speeds), may impose greater variations than those due to damage. Two approaches are generally found in the literature and in the practice of feature modelling: i) input-output, based on regression methods such as Multiple Linear Regression (MLR) [9] or ii) output-only, based on latent variable methods such as Principal Component Analysis (PCA) [10]. The first removes the effects of the EOVs, establishing relationships between measured actions (e.g., temperature, traffic, wind) and measured structural responses. When monitoring systems do not include the measurement of EOVs, latent variable methods can be employed. These methods can suppress independent actions using only structural measurements.

Data fusion focuses on reducing the volume of data while preserving its most relevant information. The fusion process may combine features from a single sensor, features from spatially distributed sensors or even heterogeneous data types. The Mahalanobis distance has been thoroughly used in this context due to its capacity to describe the variability in multivariate data sets [11].

Feature classification aims at discriminating the features into healthy or damaged. It can be divided into supervised or unsupervised learning algorithms [12]. When training data is available from both undamaged and damaged structures, supervised learning algorithms can be used, such as statistical process control [6] or MLP neural networks [13]. Since data obtained from damaged structures is rare or inexistent, unsupervised learning algorithms have been increasingly observed in the literature. Novelty detection methods are the primary class of algorithms used in this situation. This type of algorithm is a two-class problem that indicates if the acquired data comes from normal operating conditions or not. Due to its simplicity and effectiveness, outlier analysis is a broadly implemented damage detection technique [14]. In spite of the SHM feature classification resorting to clustering methods has been reported mainly following the supervised strategy of pre-defining cluster partitions to describe one or more known

structural behaviors, and subsequently compare them with new ones, this type of techniques have an unsupervised nature [15]. The major advantage of cluster-based strategies, over those previously described, consists of the greater sensitivity exhibited by these algorithms, which is related to their capacity to analyses data compactness and separation instead of defining boundaries between or around data objects. The works describing cluster-based classification for damage detection refer its high sensitivity to structural changes, and associate it with the ability of these methods to analyses compactness and separation within feature sets.

While most of SHM works rely on responses derived from ambient vibrations or static responses, recent works have also been using the structural responses generated by traffic on bridges to take advantage of the repeatability of these actions, their known behaviour, and their large magnitude, which imposes a greater excitation of the bridge in a short-time, when compared with ambient or static loads [16,17]. However, robust and effective implementations of SHM in bridges based on traffic-induced dynamic responses are still scarce. In most damage detection methodologies that have been proposed, the EOVs in the structural response are often disregarded, the type of damages is limited, or the loading scenarios are very specific, which limits their usability in real and complex bridges.

In this context, the present research work aims at implementing and validating a real-time unsupervised data-driven SHM strategy for early damage detection in railway bridges using traffic induced dynamic responses.

2 SHM procedure for early damage detection

The process of implementing a damage detection strategy involves the observation of a structure over a period of time using periodically spaced measurements, the extraction of features from these measurements, and the analysis of these features to determine the current state of health of the system [18].

A schematic representation of the proposed SHM strategy for early damage detection followed in this chapter is depicted in Fig. 2. The first step to develop a SHM strategy is to perform an operational evaluation and define a data acquisition system for the selected structure to set limitations on what will be monitored and how the monitoring will be accomplished. In this research work, a long-span bowstring-arch railway bridge was selected as case study. Section 3 details the bridge, the monitoring system installed and the undamaged and damaged scenarios considered.

In order to accomplish a fully autonomous and real-time SHM system the following four main steps regarding damage detection are implemented in section 4: i) Feature extraction, ii) Feature modelling, iii) Data fusion, and iv) Feature classification.

The feature extraction is accomplish implementing a hybrid combination of CWT and PCA to the vibration-based measurements acquired by the monitoring system installed in the railway bridge. During this step, data compression is achieved by transforming the thousands of points from each dynamic response of the structure into a few hundreds of features. Subsequently, feature modelling is performed to reduce the influence of operational and environmental conditions. A latent variable method (PCA) is

implemented to remove EOVs influence without measuring the actions, that is, based on structural measurements alone. To enhance sensitivity a pattern-level data fusion is performed afterwards by implementing a Mahalanobis distance to merge the features without losing damage related information. Finally, feature classification is performed as a data-driven approach and implementing unsupervised machine learning algorithms, namely, cluster analyses.

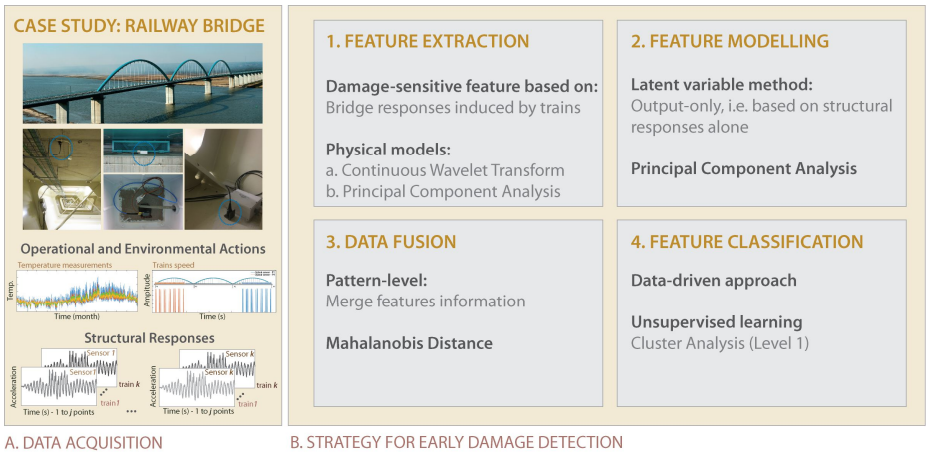

Fig. 2. Schematic representation of the SHM strategy for early damage detection.

As data-driven approaches are usually less computationally complex, they are better suited for early damage detection. Moreover, in civil engineering structures the most important question to answer is if there is or not a damage. The questions about location and severity are usually less important in this type of structures since the simple existence of damage will trigger other management procedures. For those reasons, data-driven approaches are followed in the present research with the aim of detecting damage (level 1). However, finite element models can be used to simulate damage scenarios that are not possible to obtain in any other way. These data can be then used to test the validity and robustness of the methodologies proposed for damage detection. This approach was followed and a progressive numerical model validation of the railway bridge over the Sado River was performed, in order to, afterwards, simulate damage scenarios and demonstrate the efficiency of the developed strategy.

3 Data acquisition from a bowstring-arch railway bridge

3.1 The railway bridge over the Sado River

A bowstring-arch railway bridge over the Sado River was selected as the case study used throughout this research work. It is located on the southern line of the Portuguese railway network that establishes the connection between Lisbon and Algarve (Fig. 3). The bridge is prepared for conventional and tilting passenger trains with speeds up to

250 km/h, as well as for freight trains with a maximum axle load of 25 t. Even though the bridge accommodates two rail tracks, only the upstream track is currently in operation. The bridge has a total length of 480 m, divided into 3 continuous spans of 160 m each. The bridge deck is suspended by three arches connected to each span of the deck by 18 hangers distributed over a single plane on the axis of the structure. The superstructure is composed of a steel-concrete composite deck, while the substructure, which includes the piers, the abutments and the pile foundations, is built with reinforced concrete. The deck is fixed on pier P1, whereas on piers P2, P3 and P4 only the transverse movements of the deck are restrained, while the longitudinal movements are constrained by seismic dampers.

Fig. 3. Overview of the bridge over the Sado River.

3.2 SHM monitoring system

The structural health condition of the railway bridge over the Sado River has been controlled with a comprehensive autonomous online monitoring system, as detailed in Fig. 4a, since the beginning of its life cycle. This monitoring system was defined based on an operational evaluation and allowed the acquisition of data necessary to implement the strategy for early damage detection (Fig. 2). To identify each train that crosses the bridge and compute its speed, two pairs of optical sensors were installed at both ends of the bridge (Fig. 4b). The structural temperature action is measured using PT100 thermometers and NTC thermistors. Three sections of the arch were instrumented with twelve NTC thermistors. Additionally, four NTC thermistors were fixed to the steel box girder and three PT100 thermometers were embedded in the concrete slab (Fig. 4d). To control the behaviour of the bearing devices, the responses from longitudinal displacement transducers were obtained from eight sensors, each adjacent to a bearing device (Fig. 4b). The set of sensors also includes one vertical piezoelectric accelerometer fixed at the mid span of the concrete slab, two triaxial force balance accelerometers at the thirds of the mid-span steel box girder, and twelve vertical force balance accelerometers fixed along each span of the steel box girder (Fig. 4c). Four longitudinal MEMS DC accelerometers were also installed at the top of each pier (Fig. 4b). Data acquisition is carried out continuously, at a sampling rate of 2000 Hz, by a locally deployed industrial computer to save the time history during the passage of the trains.

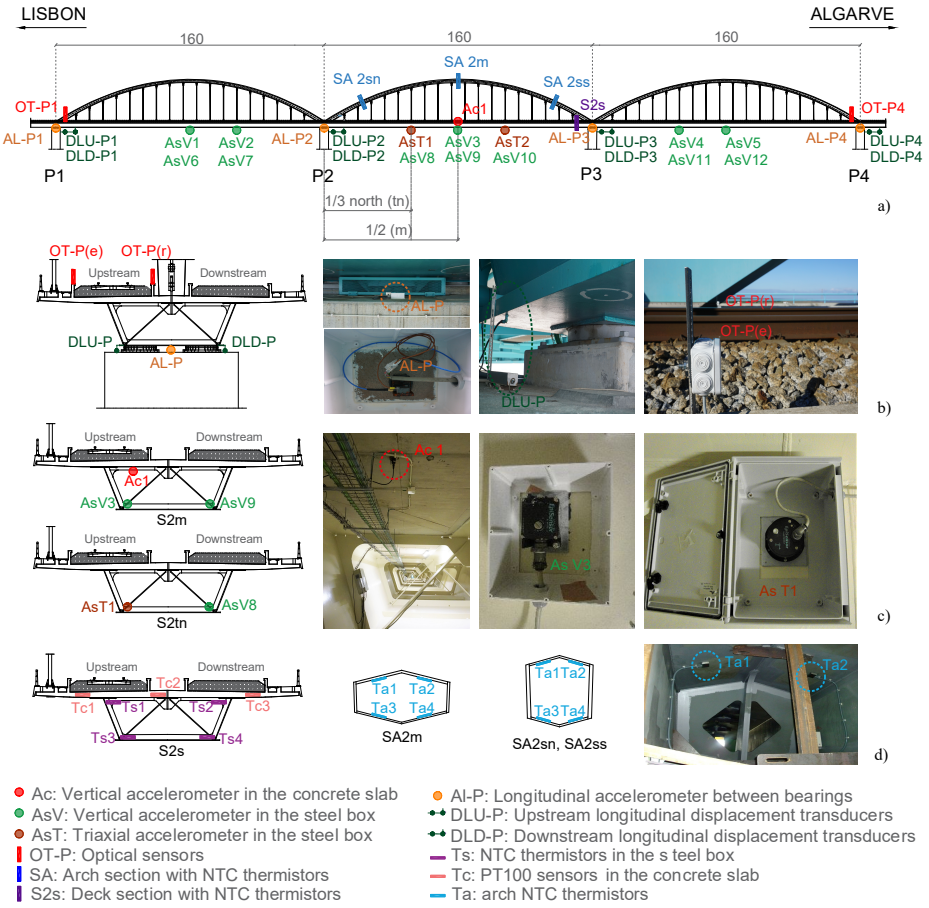

Fig. 4. SHM system installed in the railway bridge over the Sado River: a) overview, b) longitudinal accelerometer, displacement transducer and optical sensor, c) vertical and triaxial accelerometers and d) NTC thermistors and PT100 sensors.

3.3 Baseline and damage scenarios simulation

A realistic simulation of healthy and damage scenarios was conducted to test and validate the strategies proposed herein, since it was not possible to simulate damage scenarios experimentally. After a successfully validation of the methodology, it can be directly applied to experimental data from different types of bridges, where a baseline scenario is defined, and further experimental data can be tested to detect the occurrence of eventual structural changes.

For this purpose, a 3D finite element (FE) numerical model of the bridge was developed in ANSYS software [19] and fully validated with experimental data (Fig. 5). Among the modelled structural elements, those defined as beam finite elements consist of piers, sleepers, ballast-containing beams, rails, arches, hangers, transverse stiffeners, diaphragms and diagonals. Shell elements were used to model the concrete slab and the steel box girder, while the pads, the ballast layer and the foundations were modelled

using linear spring-dashpot assemblies. The mass of the non-structural elements and the ballast layer was distributed along the concrete slab. Concentrated mass elements were used to reproduce the mass of the arches' diaphragms and the mass of the sleepers, which were simply positioned at their extremities. The connection between the concrete slab and the upper flanges of the steel box girder, as well as the connection between the deck and the track, were performed using rigid links. Special attention was paid to the bearings supports, as they can strongly influence the performance of the bearings, non-linear contact elements were applied. Moreover, constraint elements located between the bearings were used to restrict the transversal movement in each pier, and the longitudinal and transversal movements in the case of the first pier.

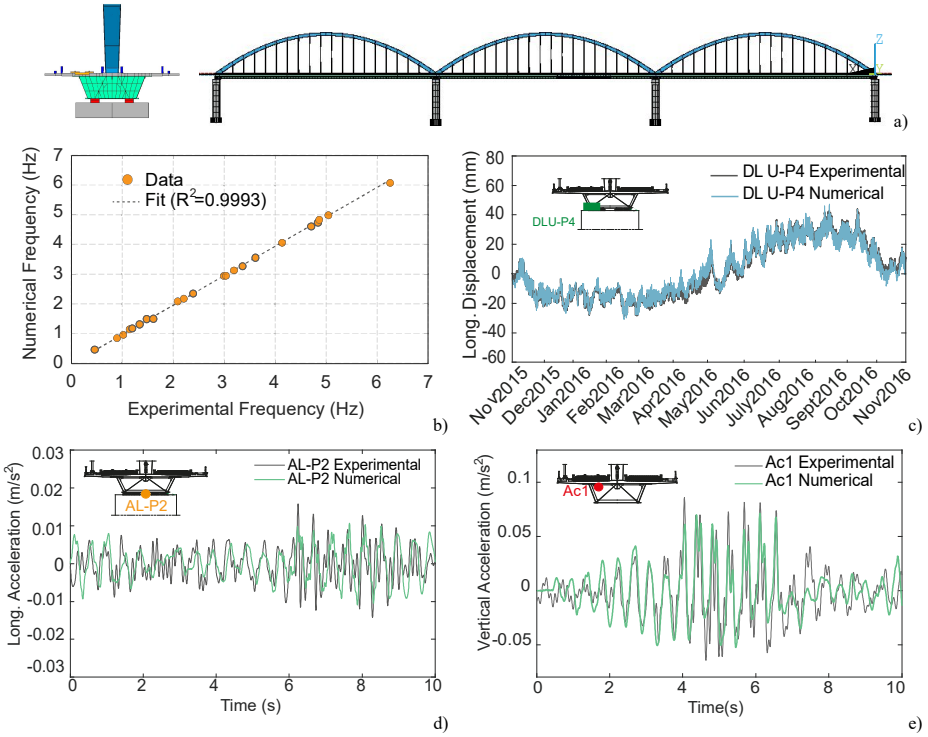

Fig. 5. Numerical modelling and validation: a) 3D FE numerical model of the bridge over the Sado River, b) agreement between numerical and experimental modal frequencies, c) static validation of the displacements measured on pier P4, c) dynamic validation of longitudinal accelerations at pier P2 with the AP at 216km/h, and d) dynamic validation of vertical accelerations at the concrete slab (Ac1) with the AP at 216km/h.

To ensure that the numerical model accurately simulates the structural behavior of the bridge, the responses obtained from modal, static and dynamic analyses were compared with those measured by the SHM system [20]. The numerical natural frequencies were compared with those obtained experimentally during an ambient vibration test [21].

Fig. 5b shows a very high coefficient of determination (R^2=0.9993) between the numerical and the experimental results. To validate the static behaviour of the numerical model, the response of the structure to the action of temperature was studied. The structural static behaviour of the bridge was simulated in the FE model by running a time-history analysis using experimental data as input. The simulation procedure consisted of using the temperatures acquired every hour on site over the course of one year. Fig. 5c presents a very good agreement between the numerical and experimental displacements of pier P4 for the temperature measured on site between November 2015 and November 2016. Regarding the dynamic behavior, numerical simulations were conducted considering the Portuguese Alfa Pendular (AP) train as a set of moving loads crossing the bridge over the Sado River at a speed of 216 km/h. Fig. 5d,e shows a very good agreement between the experimental and numerical responses, in terms of the longitudinal accelerations measured on pier P2, and the vertical accelerations acquired on the concrete slab at the second mid-span (Ac1), respectively. Before the comparison, the time-series were filtered based on a low-pass digital filter with a cut-off frequency equal to 15 Hz. A detailed description of the numerical model and its validation com be found in Meixedo et al. [20].

The dynamic numerical simulations implemented in the present research work aimed at replicating the structural quantities measured in the exact locations of the 23 accelerometers installed on site (Fig. 4) during the passage of a train in the bridge. To correctly reproduce these structural responses, the temperature action measured precisely during the passage of each train was introduced as input in the numerical model. The measurements of the optical sensors' setup were used to obtain the train speed and axle configuration, as well as the type of train [22]. The dynamic analyses mentioned hereafter were carried out for two of the passenger trains that typically cross the bridge over the Sado River, namely, the AP train and the Intercity (IC) train. Their frequent speeds on the bridge are 220 km/h for the AP train and 190 km/h for the IC train. The nonlinear problem was solved based on the Full Newton-Raphson method and the dynamic analyses were performed by the Newmark direct integration method, using a methodology of moving loads [9]. The integration time step (Δt) used in the analyses was 0.005 s.

Fig. 6a summarizes the 100 simulations of the baseline (undamaged) condition that aim at reproducing the responses of the bridge taking into account the variability of temperature, speed, loading schemes (LS) and type of train. These baseline scenarios compose the training dictionary and do not include any damage on any location. During each simulation, real temperatures measured by the SHM system were introduced in the elements of the bridge. The average values for each season were 21ºC for spring, 30ºC for summer, 16ºC for autumn and 10ºC for winter, but the dispersion across the structure was considered by measuring and using temperature values in all elements of the bridge. The simulations included the AP and IC trains crossing the bridge with ten different loading schemes, according to the experimental observations previously made by Pimentel et al. [23]. Three train speeds were considered for each type of train, as observed in Fig. 6, thus resulting in 100 time-history simulations for the baseline condition, each taking approximately 10 hours on a 4.2 GHz Quad-Core desktop with 32.0 GB of RAM.

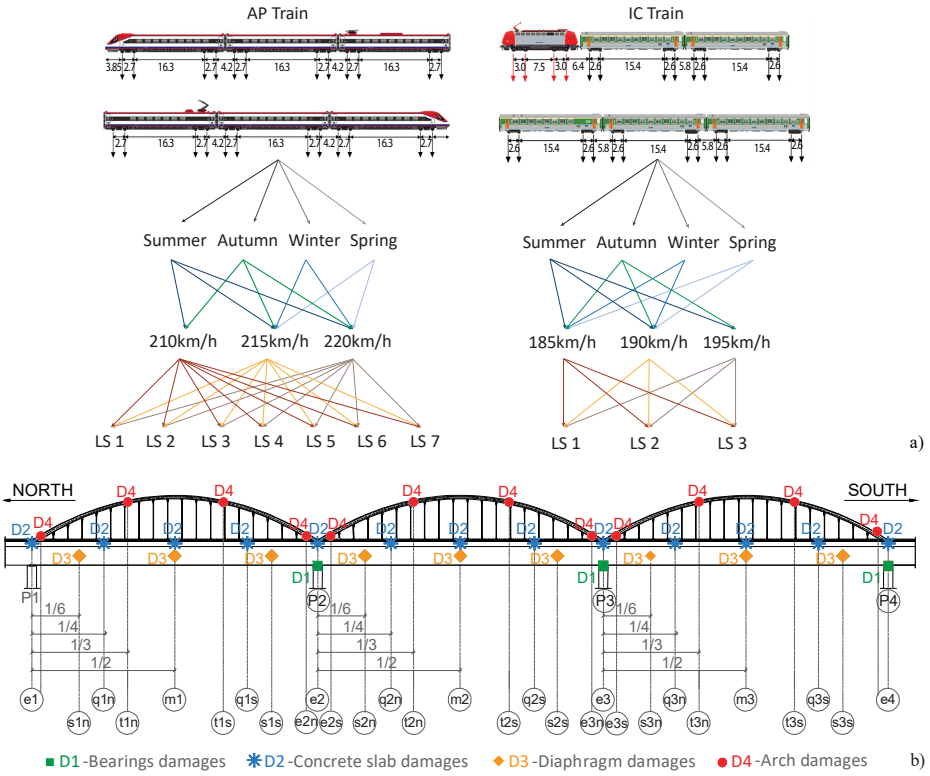

Fig. 6. Baseline and damage scenarios: a) combination of 100 simulations for the baseline condition, b) types of damages and their location on the bridge over the Sado River.

On the other hand, the damage scenarios were chosen based on possible vulnerabilities identified for the type of structural system, taken into account its materials, behavior, loadings and connections. As shown in Fig. 6b, damage scenarios were simulated according to different groups: i) damage in the bearing devices (type D1), ii) damage in the concrete slab (type D2), iii) damage in the diaphragms (type D3), and iv) damage in the arches (type D4). Each scenario was simulated considering only one damage location. Nevertheless, if, by any chance, two or more damage scenarios in different locations are observed at the same time, the effects from multiple damage locations are expected to superimpose, and the influence on the features extracted from the data will be greater. Therefore, the multiple damage scenario will be more observable than the scenarios tested here. Regarding the group of type D1, four severities of damage were included, namely, increases of the friction coefficient from a reference value of 1.5% to 1.8%, 2.4%, 3.0%, as well as to a full restrain of the movements between the pier and the deck. The remaining damage scenarios consisted of 5%, 10% and 20% stiffness reductions in the chosen sections of the bridge (Fig. 6b) on the concrete slab (D2), the diaphragms (D3), and arches (D4). These structural changes were simulated by reducing the modulus of elasticity of concrete (type D2) and of steel (types D3 and D4). A

total of 114 damage scenarios were simulated for AP train crossings at 220 km/h and adding as input the temperatures measured on site during a summer day. Additional damage scenarios could have been simulated for different combinations of EOVs. However, as observed in section 4.2, the proposed methodology is effective in removing these effects and keeping only those generated by structural changes.

The time-series illustrated in Fig. 7 are examples of simulated responses for baseline and damage conditions, acquired from the accelerometer Ac1.

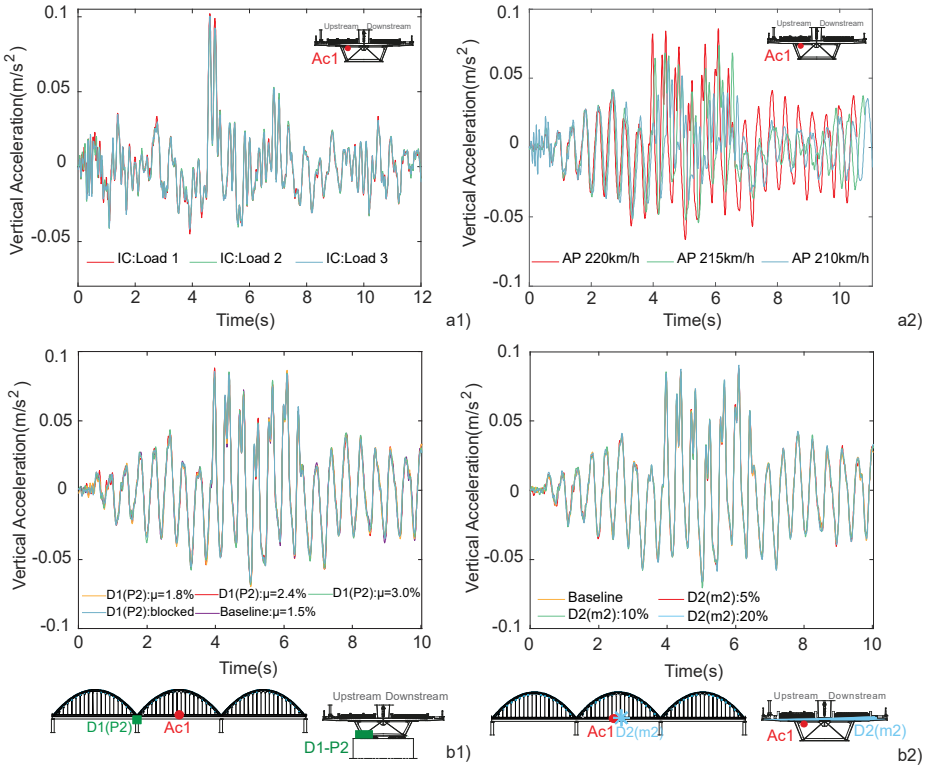

Fig. 7. Numerical simulations of sensor Ac1: a1) baseline time-series using different LS of the IC train at 190 km/h, a2) baseline time-series using different speeds of the AP train with LS5, b1) damage time-series considering friction increase D1 (P2), and b2) damage time-series considering stiffness reduction D2 (m2).

To obtain the most reliable reproduction of the real SHM data, the noise measured on site by each accelerometer was added to the corresponding numerical output. These noise distributions were acquired while no trains were travelling over the bridge and under different ambient conditions. Each simulation was corrupted with different noise signals acquired at different days, thus ensuring the most representative validation for the techniques developed herein.

The variations associated with different train types, loading schemes and train speeds are shown in Fig. 7 a1, a2. A clear distinction between the bridge responses for the IC

(Fig. 7 a1) train and the AP train (Fig. 7 a2) passages can be observed, thus displaying the necessity of considering different train types for implementing damage detection strategies. Contrariwise, Fig. 7 a1 allows observing that different LS generate smaller changes in the dynamic responses. The train speed also has an important influence in the structural response induced by trains crossing the bridge, as shown in Fig. 7 a2.

The influence of damage scenarios in the signal obtained for the train crossings appears to be much smaller than that observed for EOVs, even when regarding sensors adjacent to the damages and for the biggest magnitudes considered (20% stiffness reductions). This conclusion can be easily observed in Fig. 7 b1, b2, where the bridge responses considering friction increments in the bearing devices of pier P2 and stiffness reductions in the concrete slab are, respectively, presented.

4 Strategy for early damage detection using train induced responses

4.1 Features extraction based on CWT and PCA

The first step of the strategy is to extract damage-sensitive features based on the hybrid combination of Continuous Wavelet Transform (CWT) and Principal Component Analysis (PCA). After extracting the wavelets coefficients by applying a CWT to the acceleration measurements, a PCA is performed to significantly compress information.

Wavelet functions are composed of a family of basic functions that can describe a signal in localized time (or space) and frequency (or scale) domain. The main advantage achieved by using wavelets is the ability to perform local analysis of a signal, i.e., zooming on any interval of time or space. Signal-based damage detection techniques that involve wavelet analysis take advantage of this to be capable of revealing some hidden aspects of measured signals [24].

The CWT is a well-stablished method of implementing multiscale signal analysis. This technique will only be introduced here and the reader is referred to [25], amongst others, for a more detailed mathematical explanation. The CWT decomposes the analyzed signal into a set of coefficients in two dimensions, shift and scale, where scale is approximately inversely proportional to frequency. A basis function is translated (shift) and stretched (scale), and compared against the signal. High coefficients represent a good match between signal and wavelet at a particular instant in time and related frequency [26]. Hereupon, the CWT provides variable resolution and delivers a map of the energy content of the signal in time and frequency.

Let $f(t)$ be the acceleration response of the system, where t denotes time. The wavelet coefficients are described as the inner product of the function f and the wavelet $\psi_{a,b}$ corresponding to parameters a (scale) and b (shift) [26]:

$$W_\psi f(a,b) = \langle f, \psi_{a,b} \rangle = \frac{1}{\sqrt{a}} \int_{-\infty}^{+\infty} f(t)\, \psi^* \left(\frac{t-b}{a}\right) dt \text{ for } a > 0 \quad (1)$$

In the previous equation, $\psi(t)$ is the mother wavelet, in which the superscript asterisk indicates complex conjugation. The wavelet functions $\psi_{a,b}(t)$ are constructed by a

translated and dilated version of the mother wavelet, using the two parameters a and b (Eq. (2)). The parameter b localizes the basis function at $t = b$ and its neighborhood by windowing over a certain temporal stretch depending on the parameter, a.

$$\psi_{a,b}(t) = \frac{1}{\sqrt{a}}\psi\left(\frac{t-b}{a}\right) \text{ for } a, ba, b \in R^{+} \tag{2}$$

The frequency content can be controlled by varying the parameter a, as shown by the Fourier transform of the wavelet function (Eq. (3)). Therefore, the wavelet transform coefficient for any particular a and b characterizes the contribution to the function $f(t)$ in the neighborhood of $t = b$ and in the frequency band corresponding to the dilation factor of a.

$$\hat{\psi}_{a,b}(\omega) = \sqrt{a}\hat{\psi}(a\omega)e^{i\omega b} \tag{3}$$

Usually, the wavelet coefficients are shown in terms of scale a. However, it is common in engineering practice to work in the frequency domain. Since there is not a direct relationship between scale and frequency, the results illustrated herein are given in terms of pseudo-frequency. A pseudo-frequency f that corresponds to the scale a can be defined by Eq. (4) where Δt is the sampling period of the analyzed signal and f_c is the center frequency given by the maximizer of $|\hat{\psi}|$ [26,27].

$$f = \frac{f_c}{a\Delta t} \tag{4}$$

Considering a vector of 2112 acceleration measurement points, the present analysis used the Morlet mother wavelet [28] to extract matrices of *2112-by-82* features (wavelets coefficients) for each of the 23 sensors and for each of the 214 structural conditions. To illustrate the feature extraction procedure, Fig. 8 shows these matrices, plotted as images with scaled colours, for two different sensors: 1) AL-P2 - longitudinal accelerometer located in pier P2, 2) Ac1 - vertical accelerometer in the mid-span section of the concrete slab); and for four structural conditions: a) undamaged scenario AP|220km/h|AUT - the AP train crossing the bridge at 220 km/h during an autumn day, b) undamaged scenario IC|190km/h|SPR - the IC train crossing the bridge at 190 km/h in a spring day, c) damaged scenario D1 (P2: restrained) - the full restraint of the bearing devices in pier P2, and d) damaged scenario D2 (e2: 20%) - the 20% stiffness reduction in a section of the concrete slab aligned with pier P2.

In Fig. 8 is possible to clearly observe different energy concentrations depending on the sensor. Sensor AL-P2 seems to be more sensitive to the different structural conditions analysed, since the CWT coefficients from this sensor (Fig. 8 a1, b1, c1, d1) provide a much clearer image of the evolution of the energy content from the undamaged scenarios to the damaged scenarios. On the contrary, the energy concentration on the images from sensor Ac1 seems to be very similar between the undamaged scenario AP|220km/h|AUT (Fig. 8 a2) and both damage scenarios D1 and D2 (Fig. 8 c2, d2). The main variation in frequency values is observed for the undamaged scenario IC|190km/h|SPR (Fig. 8 b2), which indicates that the influence of varying environmental and operational conditions (such as different temperature, train and speed) may be

greater than the damage occurrence. These results also show that different sensors can store different information about the bridge structural condition, thus, combining this information may enhance the features sensitiveness.

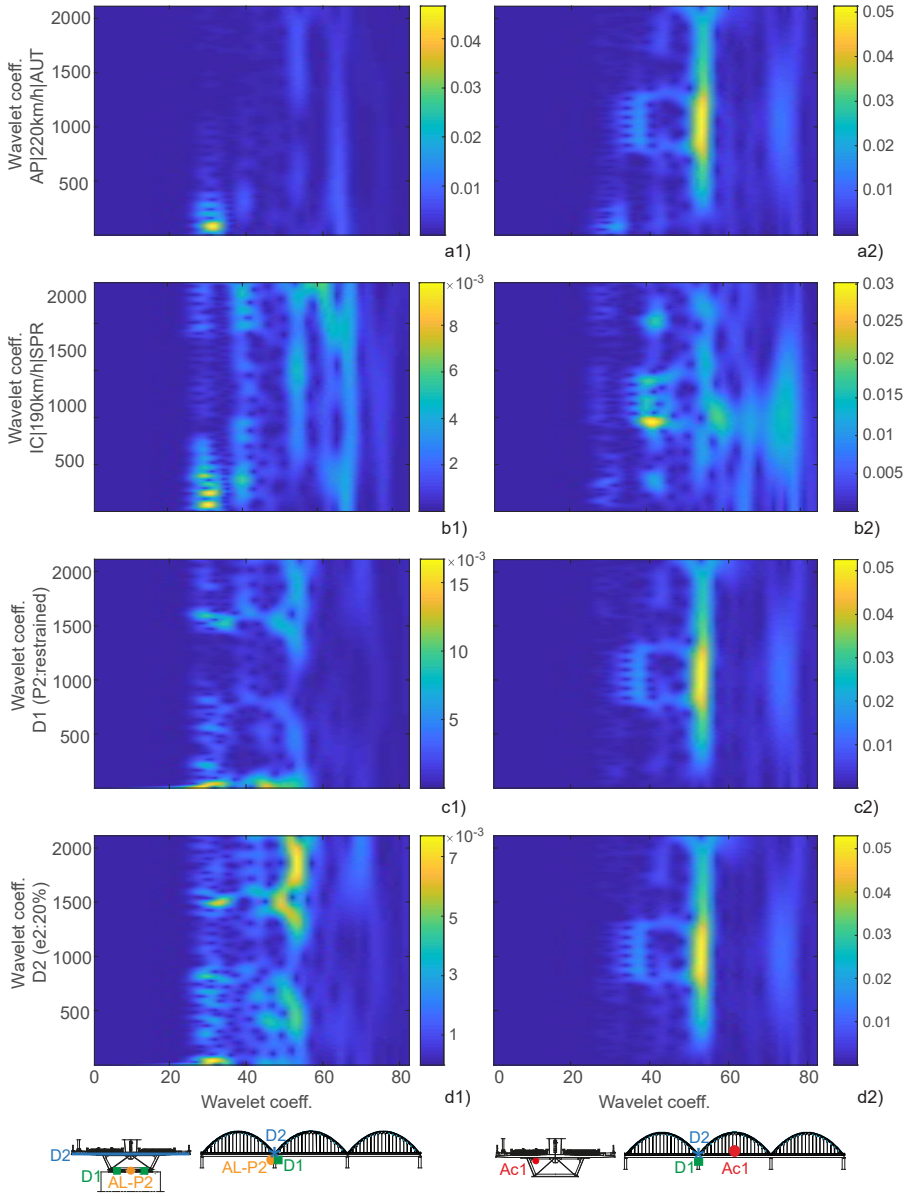

Fig. 8. Wavelet coefficients extracted from the acceleration responses according to the structural condition of the bridge and the sensor location.

PCA is a multivariate statistical method that produces a set of linearly uncorrelated vectors called principal components, from a multivariate set of vector data [29]. This operation intends to extract damage-sensitive features from the CWT coefficients while performing important data compression. Considering an *n-by-m* matrix X with the wavelets coefficients obtained after the CWT implementation, being in this case study $n=2112$ and $m = 82$, a transformation to another set of m sensors, Y, designated principal components or scores, can be achieved by the following equation:

$$Y = X \cdot T \tag{5}$$

where T is an *m-by-m* orthonormal linear transformation matrix that applies a rotation to the original coordinate system. The covariance matrix of the measurements, C, is related to the covariance matrix of the scores, Λ, as follows:

$$C = T \cdot \Lambda \cdot T^T \tag{6}$$

in which T and Λ are matrixes obtained by the singular value decomposition of the covariance matrix C. The columns of T are the eigenvectors and the diagonal matrix Λ comprises the eigenvalues of the matrix C in descending order. Hence, the eigenvalues stored in Λ are the variances of the components of Y and express the relative importance of each principal component in the entire data set variation [30].

To allow data compression, four statistical parameters, namely the root mean square (RMS), the standard deviation, the Skewness and the Kurtosis, are afterwards extracted from the scores, Y. Thereby, the information presented in a matrix of *2112-by-82* is transformed into a matrix of *4-by-82*. A total of 328 features are thus extracted from each of the 23 accelerometers. This operation is implemented for each of the 214 structural conditions.

Four of the 328 features (12, 47, 116, and 323) obtained for two of the 23 sensors, AL-P2 and Ac1, are represented in Fig. 9. These features are divided according to the structural condition in two main groups: baseline (first 100 simulations) and damage (subsequent 114 simulations). The main changes in the amplitudes of the features are induced by the type and speed of the trains. In addition, for each speed value, the changes observed in the amplitude of the statistical parameters are generated by changes in the structural temperature values (chosen for autumn, spring, summer or winter). The different LS (the seven symbols in a row in the case of the AP and three symbols in a row in the case of the IC) considered for each train type and speed, and each temperature, are the operational factors with the smallest influence on the feature variability regarding the baseline simulations. The analysis of the features shown in Fig. 9 allow drawing some conclusions about the difficulty in distinguishing undamaged and damage scenarios, since the variations caused by environmental and operational effects result in similar or greater changes in the parameters.

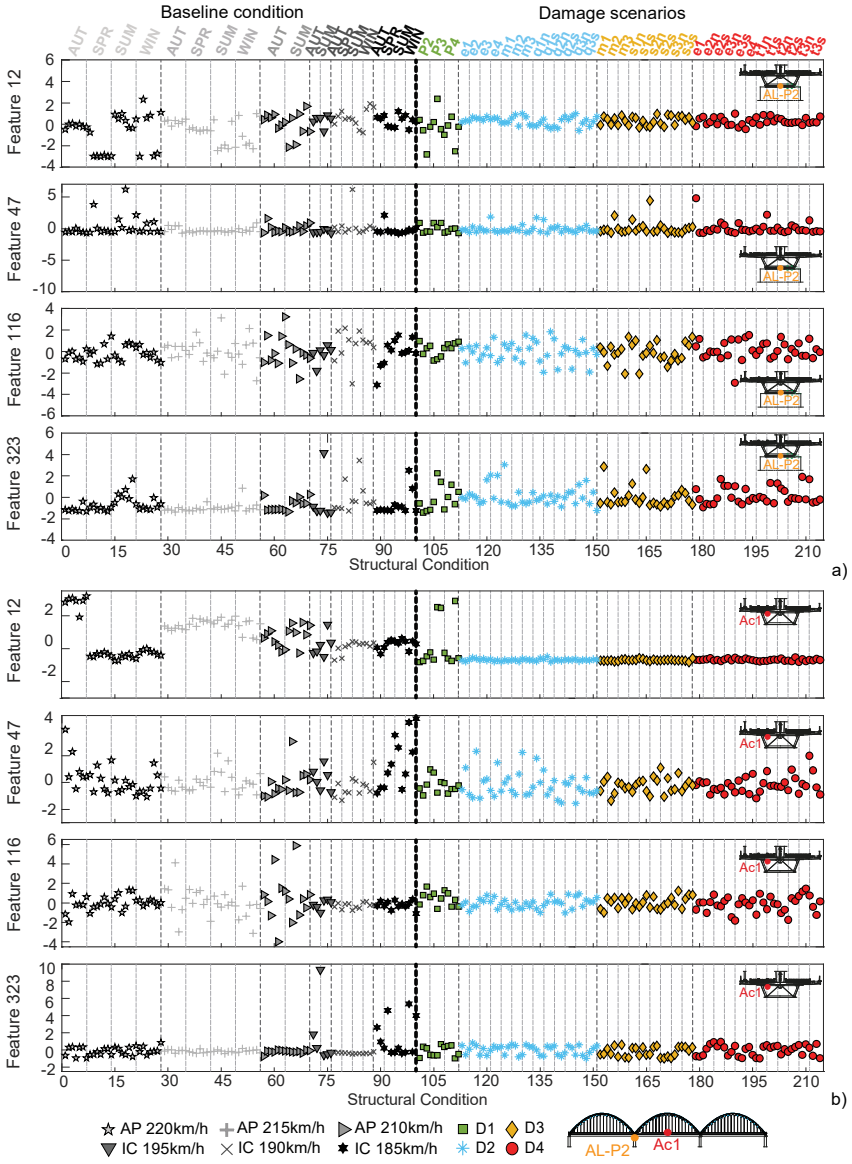

Fig. 9. Amplitude of four of the 328 statistical features extracted based on CWT and PCA, for all 214 structural conditions and from two of the 23 sensors: a) longitudinal accelerometer located on pier P2 (AL-P2), b) vertical accelerometer located in the mid-span section of the concrete slab (Ac1).

4.2 Features modelling based on PCA

The analysis of the features presented in Fig. 9 revealed the necessity to adequately model these statistical parameters to remove the changes generated by EOVs and highlight those generated by damage. Assuming that environmental conditions have a linear effect on the identified features, the implementation of a latent variable method as PCA to the extracted features may efficiently remove environmental and operational effects, without need to measure these actions [11,30].

Considering now an *n-by-m* matrix X with the features extracted from the dynamic responses, where n is the number of simulations for the baseline condition (i.e., 100 in this case study) and m is the number of features from all the sensors (i.e. 328), a transformation to another set of m parameters, Y, can be achieved by applying Eq. (5).

As demonstrated by Santos et al. [10], the PCA is able to cluster meaningful information related to EOVs in the first components, while variations related to other small-magnitude effects, such as early-damage, may be retained in latter components. Since the purpose of the present research work is to detect damage, which has generally a local character, the feature modelling operation consists of eliminating the most important principal components (PCs) from the features and retaining the rest for subsequent statistical analysis. Bearing this in mind, the matrix Λ from Eq. (6) can be divided into a matrix with the first e eigenvalues and a matrix with the remaining *m-e* eigenvalues. Defining the number of e components remains an open question with regard to the representation of the multivariate data; although several approaches have been proposed, there is still no definitive answer. In this work, the value of e (or the number of PCs to discard) is determined based on a rule of thumb in which the cumulative percentage of the variance reaches 80% [31]. After choosing e, the *m-e* components of the matrix Y can be calculated using Eq. (5) and a transformation matrix $\hat{T}$ built with the remaining *m-e* columns of T. Those *m-e* components can be remapped to the original space using the following:

$$F_{PCA} = X \cdot \hat{T} \cdot \hat{T}^T \tag{7}$$

where F_{PCA} is the *n-by-m* matrix of CWT-double PCA-based features, expected to be less sensitive to environmental and operational actions and to be more sensitive to the damage scenarios. This procedure is repeated for each sensor.

Since the cumulative percentage of the variance of the sum of the first nine principal components was higher than 80% for different structural conditions, these nine PCs were discarded during the modelling process (i.e., $e = 9$). Fig. 10 shows the series of four features (12, 47, 116 and 323) across the 214 scenarios obtained for AL-P1 and Ac1 accelerometers, after the application of the double PCA. The direct comparison of these action-free damage-sensitive features with those shown before the feature modelling (Fig. 9) allows observing that, in fact, the feature modelling enabled removing the variations generated by the temperature, as well as by the type and speed of the train, but not those generated by damage. Moreover, the features sensitivity to the damage scenarios was increased.

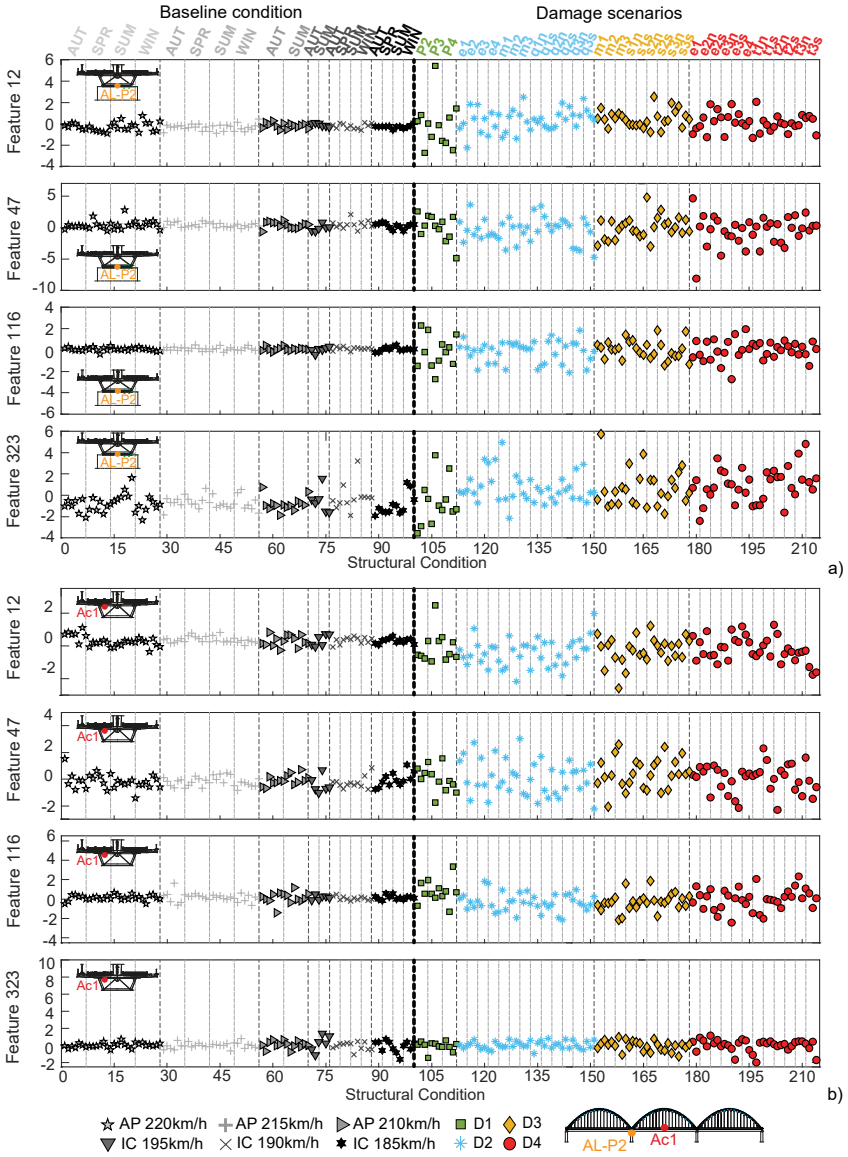

Fig. 10. Amplitude of four of the 328 features modelled based on PCA, for all 214 structural conditions and from two of the 23 sensors: a) longitudinal accelerometer located on pier P2 (AL-P2), b) vertical accelerometer located in the mid-span section of the concrete slab (Ac1).

4.3 Features fusion

To improve the features' discrimination sensitivity, data fusion was performed. A Mahalanobis distance was implemented to the modelled features in order to describe their variability and allowing their effective fusion.

The Mahalanobis distance measures the distance between the baseline features and the damage-sensitive features to express the similarities between them, with shorter distances representing greater similarities. The Mahalanobis distance is generic enough to be used to detect any damage scenario, while providing a weighting that is entirely unsupervised, and therefore independent of human intervention, the type of structure, and the actions imposed on it. It consists of a weighted damage indicator in which the weights are determined by the covariance structure. In addition, and more importantly, the weighting proportional to the covariance structure provides an additional layer of feature modelling which, when defined for regular actions, allows outlining with high sensitivity those that were not used for the definition of the covariance structure. The analytical expression of the Mahalanobis distance for each simulation i, denoted as MD_i, is the following:

$$\mathrm{MD_i} = \sqrt{(\mathrm{x_i} - \bar{\mathrm{x}}) \cdot \mathrm{S_x}^{-1} \cdot (\mathrm{x_i} - \bar{\mathrm{x}})^{\mathrm{T}}} \tag{8}$$

where x_i is a vector of m features representing the potential damage/outlier, $\bar{x}$ is the matrix of the means of the features estimated in the baseline simulations, and S_x is the covariance matrix of the baseline simulations.

The Mahalanobis distance is computed for each simulation and each sensor resulting in a matrix with n Mahalanobis distances for k sensors, where n is the total number of structural conditions. When data from a structural state that differs from the baseline is tested, the MD value is expected to increase substantially.

Hence, the Mahalanobis distance allowed transforming, for each sensor and train crossing, the 328 features into one single feature (a distance in the feature space), which exhibits higher values for different structural conditions and null (or near-null) values for identical structural scenarios. The outcome of this procedure is a vector of *214-by-1,* of distances, one for each of the 23 sensors.

Fig. 11 shows the results achieved for two of the 23 sensors (AL-P2 and Ac1). The two plots in Fig. 11 clearly show the difference in sensitivity for different sensors in each structural condition. The longitudinal accelerometer on pier P2 (Fig. 11a) is more sensitive to damages on the bearing devices of piers P3 and P4. Conversely, the accelerometer located at the second mid-span of the concrete slab (Fig. 11b) exhibits an important global sensitivity to damage, since there is a distinction between the baseline simulations and the damage scenarios, but it is not efficient in distinguish the different types of simulated damages.

4.4 Clustering-based classification

Time-series analysis and distance measures can help perform data analysis and suggest the existence of different structural behaviours within a data set, as shown in the previous sections. However, the development of real-time SHM strategies should resort to machine learning algorithms that can autonomously decide whether one or more distinct structural behaviours are being observed from patterns in the features. Hence, feature discrimination is addressed herein using unsupervised classification algorithms.

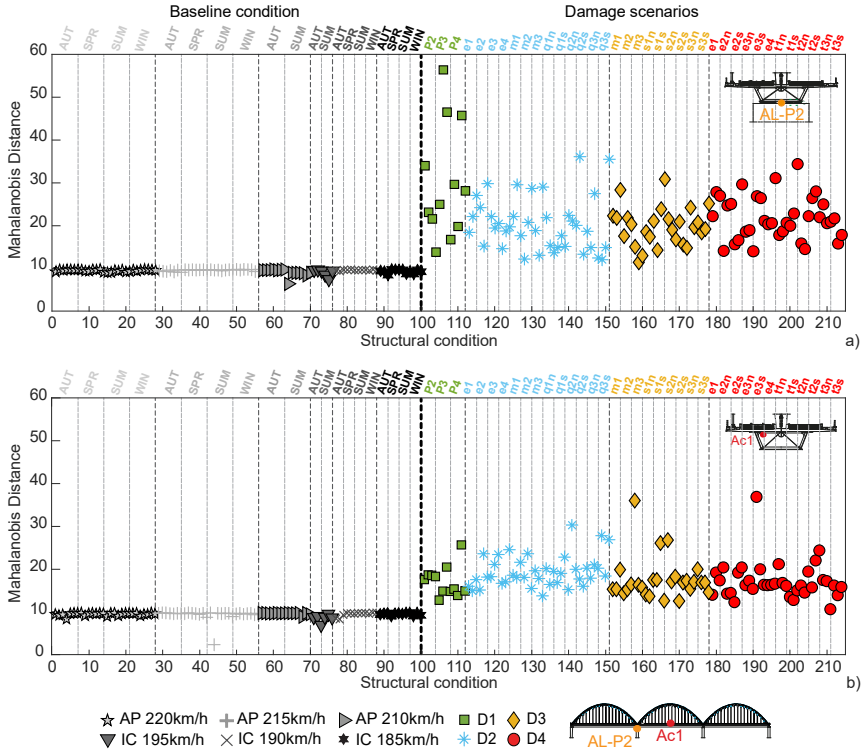

Fig. 11. Features fusion based on the Mahalanobis distance for all 214 structural conditions, considering the responses from accelerometers: a) AL-P2, b) Ac1.

Cluster analysis was the data mining technique chosen to address feature classification. The aim of the clustering process is to divide a dataset into groups, which must be as compact and separate as possible. This can be mathematically posed as an attempt to minimize the dissimilarity between features assigned to the same cluster (within-cluster distance), which, consequently, maximizes the dissimilarity between the features assigned to different clusters (between-cluster distance) [15]. Considering a given partition containing K clusters, $P_k = \{C_1, \dots, C_k\}$, the overall within-cluster dissimilarity $W(P_k)$ and the overall dissimilarity OD can be defined as:

$$\mathrm{W(P_k)} = \frac{1}{2}\sum_{\mathrm{k=1}}^{\mathrm{K}} \sum_{\mathrm{c(i)=k}} \sum_{\mathrm{c(j)=k}} \mathrm{d_{ij}} \tag{9}$$

$$\mathrm{OD} = \frac{1}{2}\sum_{\mathrm{i=1}}^{\mathrm{N}} \sum_{\mathrm{j=1}}^{\mathrm{N}} \mathrm{d_{ij}} \tag{10}$$

in which the between-cluster dissimilarity is given by the subtraction $B(P_k) = OD - W(P_k)$. Here, N is the total number of features and $c(i)$ is a many-to-one allocation

rule that assigns feature i to cluster k, based on a dissimilarity measure d_{ij} defined between each pair of features i and j. The best-known clustering algorithm is iterative and called k-means [32]. The k-means requires that the number of $K < N$ clusters be initially defined along with a randomly defined set of K clusters' prototypes. This task is called initialization. Afterwards, each iteration starts by allocating the features to the clusters according to an allocation rule, $c(i)$, that assigns each feature to the least dissimilar (closest) cluster prototype. The second step of each k-means' iteration is called representation and consists of defining the centroids of the K clusters as their prototypes and assuming that each feature belongs to the cluster whose prototype is closest. These two steps, allocation and representation, are subsequently repeated until an objective function, which depends on the compactness and separation of the cluster, reaches its global minimum value. The k-means considers the squared within-cluster dissimilarity measured across the K clusters as an objective function [32]. Clusters' dissimilarities are generally defined as distance metrics. Among these, the Euclidean (square root of the sum-of-squares) is used here.

As previously mentioned, the k-means clustering method requires that the number of clusters be defined in advance and provided as input (in the initialization phase). For damage detection, there is no way of knowing this number in advance, which requires that multiple partitions, comprising different numbers of clusters, be tested and their outcomes analyzed using cluster validity indices [32]. Numerous validity indices have been proposed and tested, not only in specific literature but also in SHM applications. Herein, the global silhouette index (SIL) is used, since it revealed a superior performance in previous studies [33], in which its formulation is carefully described.

The application of the k-means along with the SIL index is exemplified here using the features extracted from the sample time-series. For the present work, it is important to note that, among the K tested, the partition that generates the highest SIL value is the one that is expected to best describe the analyzed feature set, and should, therefore, be considered for SHM purposes. Using the CWT-double PCA-based features after fusion from all sensors installed on site, the SIL indices extracted from five cluster partitions, shown with 'o' marks in Fig. 12a, exhibit a maximum for $k = 2$ clusters. The corresponding features' allocations were automatically generated by the k-means method and are shown in Fig. 12b for three of the 23 sensors: i) AL-P2, ii) Ac1, and iii) AsV4. These plots demonstrate that the clustering method can divide the features without any human interaction or input. In Fig. 12b can be observed the dissimilarity between the two centroids of three different combinations of sensors, while the plots in the diagonal of this figure show that the two clusters found for each couple of sensors are compact over time and separated when the simulated damages start. This result undeniably shows that the k-means method is capable of analyzing the feature set and, in a fully automated manner, separating it according to the structural conditions observed on site. Also, it is demonstrated that the clusters have de advantage of allowing a multidimensional representation of the features, which, in this case study, led to a classification without false detections.

After the definition of the baseline, which can be promptly achieved after one day of trains crossings, each new train crossing can be used to test the bridge structural condition based on the proposed strategy

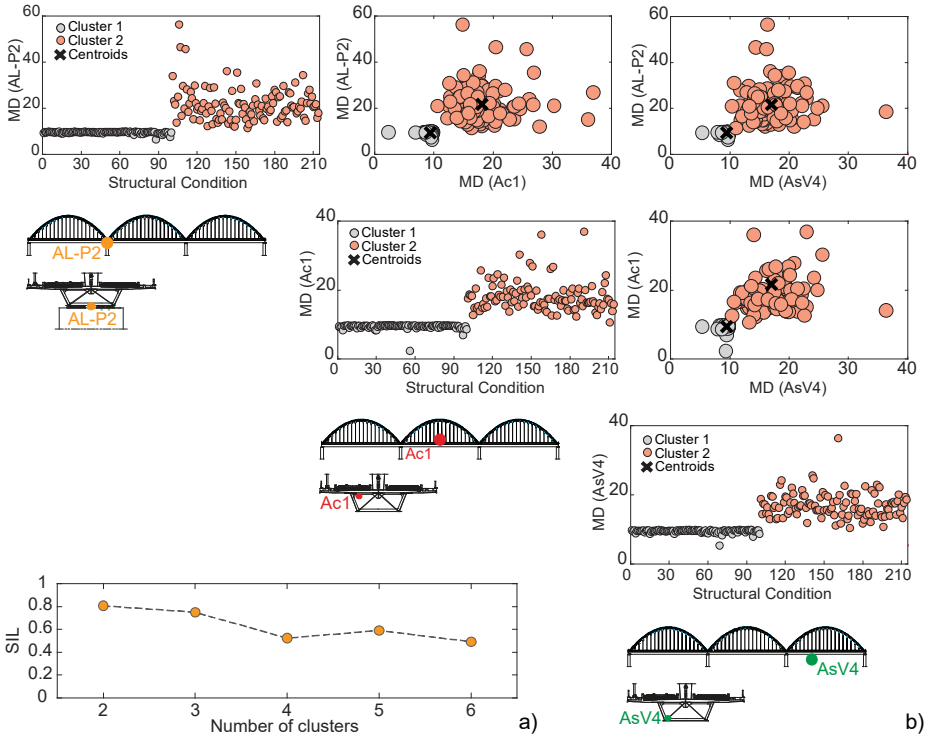

Fig. 12. Allocation of damage-sensitive features into clusters: a) silhouette index (SIL), b) clusters defined for all structural conditions and their centroids for three of the 23 sensors.

5 Conclusions

This research presents a data-driven AI-based SHM strategy for conducting real-time unsupervised early damage detection in railway bridge vibration response from traffic induced excitation, applying time series analysis and machine learning techniques. The strategy consists of fusing sets of acceleration measurements to improve sensitivity and combines: i) CWT and PCA for feature extraction, ii) PCA for feature modelling, iii) Mahalanobis distance for feature fusion, and iv) clustering algorithms for feature classification. A comprehensive dataset of baseline and damaged scenarios was simulated using a highly reliable digital twin of the Sado Bridge tuned with experimentally obtained actions as input, namely temperature, train loadings and speeds. Damage severities of 5%, 10% and 20% stiffness reductions in the concrete slab, diaphragm, and arches were simulated, as well as friction increases in the movements of the bearing. The damage-sensitive features were extracted from the bridge accelerations induced by train crossings by combining CWT with PCA. The wavelets coefficients were first extracted from the time-series. Afterwards, PCA was implemented to the wavelets coefficients and statistical parameters were extracted from the PCs to allow data compression. The study of the wavelet-PCA-based features extracted from different structural

conditions allowed drawing conclusions about the supremacy of the EOVs when compared with damage, proving the importance of feature modelling. Moreover, the information obtained from each feature was different depending on the sensor location and the statistical parameter. PCA was once again implemented to modelling the features. This latent variable method proved its importance and effectiveness in removing observable changes induced by variations in train speed or temperature without the need to measure them and without losing sensitivity to damage. To describe the variability present in the modelled features, a Mahalanobis distance was implemented to the 328 features extracted from each sensor signal. This implementation allowed corroborated that different sensors have greater or lesser sensitivity, depending on the location of the damage. Moreover, this step proved to be crucial to achieve the highest possible level of information fusion and to obtain a clear distinction between undamaged and damaged conditions. In order to automatically detect the presence of damage, a clustering-based classification was performed. The robustness and effectiveness of the proposed strategy was demonstrated by automatically detecting the damage scenarios as different from those belonging to undamaged structural conditions. Using features modelled based only on structural responses, no false detections occurred. An additional important conclusion obtained from this work is that, even with an SHM system not capable of measuring EOVs, it is possible to successfully detect different types of damage using the bridge's responses to train crossings. This achievement renders the strategy the ability to be less dependent on spatial actions very difficult to characterize, thus contributing for the normalization of SHM procedures. This strategy also has the advantages of minimizing the number of sensors that need to be installed and, consequently, the cost of the SHM system, as well as allowing for a more automatic and straightforward implementation.

Acknowledgments

This work was financially supported by the Portuguese Foundation for Science and Technology (FCT) through the PhD scholarship SFRH/BD/93201/2013. The authors would like to acknowledge the support of the R&D project RISEN through the H2020|ES|MSC - H2020|Excellence Science|Marie Curie programme, the Portuguese Road and Railway Infrastructure Manager (I.P), the Portuguese National Laboratory for Civil Engineering (LNEC), and the Base Funding - UIDB/04708/2020 of the CONSTRUCT - Instituto de I&D em Estruturas e Construções - financed by national funds through the FCT/MCTES (PIDDAC).

References

1. Melo LRT, Ribeiro D, Calçada R, Bittencourt TN. Validation of a vertical train – track – bridge dynamic interaction model based on limited experimental data. *Structure and Infrastructure Engineering* 2020; **16**(1): 181–201. DOI: 10.1080/15732479.2019.1605394.
2. Meixedo A, Ribeiro D, Calçada R, Delgado R. Global and Local Dynamic Effects on a Railway Viaduct with Precast Deck. *Proceedings of the Second International*

Conference on Railway Technology: Research, Development and Maintenance, Civil-Comp Press, Stirlingshire, UK: 2014. DOI: 10.4203/ccp.104.77.

3. Rytter A. *Vibrational Based Inspection of Civil Engineering Structures*. Aalborg: Dept. of Building Technology and Structural Engineering, Aalborg University: 1993.
4. Meixedo A, Alves V, Ribeiro D, Cury A, Calçada R. Damage identification of a railway bridge based on genetic algorithms. *Maintenance, Monitoring, Safety, Risk and Resilience of Bridges and Bridge Networks - Proceedings of the 8th International Conference on Bridge Maintenance, Safety and Management, IABMAS 2016*, Foz Do Iguaçu; Brazil: 2016.
5. Cury A, Cremona C. Assignment of structural behaviours in long-term monitoring : Application to a strengthened railway bridge. *Structural Health Monitoring* 2012; **11**(4): 422–441. DOI: 10.1177/1475921711434858.
6. Posenato D, Kripakaran P, Smith IFC. Methodologies for model-free data interpretation of civil engineering structures. *Computers & Structures* 2010; **88**(7–8): 467–482. DOI: 10.1016/j.compstruc.2010.01.001.
7. Meixedo A, Santos J, Ribeiro D, Calçada R, Todd M. Damage detection in railway bridges using traffic-induced dynamic responses. *Engineering Structures* 2021; **238**(112189). DOI: 10.1016/j.engstruct.2021.112189.
8. Mujica LE, Gharibnezhad F, Rodellar J, Todd M. Considering temperature effect on robust principal component analysis orthogonal distance as a damage detector. *Structural Health Monitoring* 2020; **19**(3): 781–795. DOI: 10.1177/1475921719861908.
9. Cavadas F, Smith IFC, Figueiras J. Damage detection using data-driven methods applied to moving-load responses. *Mechanical Systems and Signal Processing* 2013; **39**(1–2): 409–425. DOI: 10.1016/j.ymssp.2013.02.019.
10. Santos JP, Crémona C, Orcesi AD, Silveira P. Multivariate statistical analysis for early damage detection. *Engineering Structures* 2013; **56**: 273–285. DOI: 10.1016/j.engstruct.2013.05.022.
11. Hu W hua, Moutinho C, Caetano E, Magalhães F, Cunha Á. Continuous dynamic monitoring of a lively footbridge for serviceability assessment and damage detection. *Mechanical Systems and Signal Processing* 2012; **33**(November): 38–55. DOI: 10.1016/j.ymssp.2012.05.012.
12. Farrar CR, Worden K. *Structural Health Monitoring: a machine learning perspective*. Wiley, pp. 1-45; 2013.
13. Lautour OR De, Omenzetter P. Damage classification and estimation in experimental structures using time series analysis and pattern recognition. *Mechanical Systems and Signal Processing* 2010; **24**(5): 1556–1569. DOI: 10.1016/j.ymssp.2009.12.008.
14. Gonzalez I, Karoumi R. BWIM aided damage detection in bridges using machine learning. *Journal of Civil Structural Health Monitoring* 2015; **5**(5): 715–725. DOI: 10.1007/s13349-015-0137-4.
15. Cardoso R, Cury A, Barbosa F. Automated real-time damage detection strategy using raw dynamic measurements. *Engineering Structures* 2019; **196**(109364). DOI: 10.1016/j.engstruct.2019.109364.
16. Azim R, Gül M. Damage detection of steel girder railway bridges utilizing operational vibration response. *Structural Control and Health Monitoring* 2019; **26**(e2447): 1–15.

DOI: 10.1002/stc.2447.

17. Nie Z, Lin J, Li J, Hao H, Ma H. Bridge condition monitoring under moving loads using two sensor measurements. *Structural Health Monitoring* 2019; **19**(3): 917–937. DOI: 10.1177/1475921719868930.
18. Farrar CR, Doebling SW, Nix D a. Vibration–based structural damage identification. *Philosophical Transactions of the Royal Society of London A: Mathematical, Physical and Engineering Sciences* 2001; **359**(1778): 131–149. DOI: 10.1098/rsta.2000.0717.
19. ANSYS. Academic Research. Release 17.1 2016.
20. Meixedo A, Ribeiro D, Santos J, Calçada R, Todd M. Progressive numerical model validation of a bowstring-arch railway bridge based on a structural health monitoring system. *Journal of Civil Structural Health Monitoring* 2021; **11**(2): 421–449. DOI: 10.1007/s13349-020-00461-w.
21. Min X, Santos L. *Ensaios dinâmicos da ponte ferroviária sobre o rio sado na variante de alcácer*. Lisboa [Portuguese]: 2011.
22. Meixedo A, Gonçalves A, Calçada R, Gabriel J, Fonseca H, Martins R. On-line Monitoring System for Tracks. *exp.at 2015 - 3rd Experiment International Conference*, Sao Miguel Island, Azores: 2016. DOI: 10.1109/EXPAT.2015.7463240.
23. Pimentel R, Ribeiro D, Matos L, Mosleh A, Calçada R. Bridge Weigh-in-Motion system for the identification of train loads using fiber-optic technology. *Structures* 2021; **30**(November 2020): 1056–1070. DOI: 10.1016/j.istruc.2021.01.070.
24. Ren W xin, Sun Z shou. Structural damage identification by using wavelet entropy. *Engineering Structures* 2008; **30**: 2840–2849. DOI: 10.1016/j.engstruct.2008.03.013.
25. Cohen A, Ryan RD. *Wavelets and Multiscale Signal Processing*. London: Chapman & Hall, Boundary Row; 1995.
26. Cantero D, Ülker-kaustell M, Karoumi R. Time – frequency analysis of railway bridge response in forced vibration. *Mechanical Systems and Signal Processing* 2016; **76**–**77**: 518–530.
27. Ülker-kaustell M, Karoumi R. Influence of non-linear stiffness and damping on the train-bridge resonance of a simply supported railway bridge. *Engineering Structures* 2012; **41**: 350–355. DOI: 10.1016/j.engstruct.2012.03.060.
28. Teolis A. *Computational signal processing with wavelets*. Birkhauser: 1998.
29. Ribeiro D, Leite J, Meixedo A, Pinto N, Calçada R, Todd M. Statistical methodologies for removing the operational effects from the dynamic responses of a high-rise telecommunications tower. *Structural Control and Health Monitoring* 2021; **28**(4): e2700. DOI: 10.1002/stc.2700.
30. Yan A, Kerschen G, Boe P De, Golinval J. Structural damage diagnosis under varying environmental conditions — Part I : A linear analysis. *Mechanical Systems and Signal Processing* 2005; **19**(4): 847–864. DOI: 10.1016/j.ymssp.2004.12.002.
31. Jolliffe IT. Principal Component Analysis. 2nd ed., New York: Springer, pp. 112-147; 2002.
32. Hastie T, Tibshirani R, Friedman J. *The Elements of Statistical Learning, Data Miningm Inference, and Prediction*. 2nd ed. Stanford, USA: Springer, pp. 460-462; 2011.
33. Santos J, Crémona C, Calado L. Real-time damage detection based on pattern recognition. *Structural Concrete 17* 2016; **17**(3): 338–354. DOI: 10.1002/suco.201500092.